Earth and Planetary Science Letters 584 (2022) 117509

Contents lists available at ScienceDirect

Earth and Planetary Science Letters

www.elsevier.com/locate/epsl

Isotopes track Tethyan seamount subduction beneath the Troodos spreading centre, Cyprus

Rex N. Taylor [a,*], Osamu Ishizuka [d,b,c], Isabel Hessey [a], Agnes Michalik [a], Lauren Stillwell [a], Stephen White [a]

[a] School of Ocean and Earth Science, University of Southampton, Waterfront Campus, Southampton, SO14 3ZH, UK
[b] Institute of Earthquake and Volcano Geology, Geological Survey of Japan, AIST, Central 7, 1-1-1, Higashi, Tsukuba, Ibaraki 305-8567, Japan
[c] Japan Agency for Marine-Earth Science and Technology, 2-15 Natsushima, Yokosuka, Kanagawa 237-0061, Japan
[d] Geological Survey of Japan, AIST, Central 7 1-1-1 Higashi, Tsukuba, Ibaraki, 305-8567, Japan

ARTICLE INFO

Article history:
Received 20 December 2021
Received in revised form 7 March 2022
Accepted 16 March 2022
Available online 7 April 2022
Editor: L. Coogan

Keywords:
Troodos
Pb isotopes
subduction fluids
seamount collision

ABSTRACT

Supra-subduction zone volcanoes record the chemical transfer of sedimentary and igneous material from the subducting plate to the overlying mantle and lithosphere. This transfer is thought to preferentially involve fluid-mobile elements, which swamp the signature of similar trace elements in the supra-subduction mantle. Using high-resolution isotope measurements of fluid-mobile Pb, we have traced the evolution and inputs beneath the supra-subduction spreading ridge that is now the Troodos Ophiolite, Cyprus. It is apparent that variable but significant amounts of Pb are actually derived from the mantle wedge, and substantial amounts of the fluid-immobile elements like Nb are introduced from the slab. Our study identifies a chemical transformation of the spreading crust, which reflects a spatial change in the Neo-Tethyan slab. The west was influenced by the subduction of pelagic/carbonate sediments overlying MORB, whereas the east and south also include a high $^{206}Pb/^{204}Pb$ component, similar to high-μ mantle plumes distributed around northern Africa. This chemo-tectonic switch is interpreted to represent the location of supra-subduction spreading relative to the path of a seamount chain colliding with and subducting beneath the Troodos trench. The Hecataeus Rise, located to the southeast of Cyprus, is a candidate to be a foundered relic of this seamount chain, locked in the subduction zone. We also demonstrate that the supra-subduction mantle wedge was of an Atlantic/Pacific-type composition, but the subducting Neo-Tethyan oceanic crust had an Indian Ocean signature. As such, this destructive plate boundary can be defined as the Cretaceous interface between the Atlantic and Indian mantle domains.

1. Introduction

Active intra-oceanic supra-subduction spreading is generally submarine, which makes detailed sampling of a wide geographic area with stratigraphic control challenging and cost-prohibitive. This limits the potential to identify and constrain spatial and temporal chemical variations in volcanism, which are required to understand the progressive interaction between subducted lithosphere and the overlying mantle. However, a potential analogue for this tectonic environment is the Troodos ophiolite, which is an extensive emergent tract of crust (125 x 35 km) formed by Late Cretaceous spreading, and contains all lithological units expected of ocean crust (Gass, 1968). Having escaped high-grade metamorphism, Troodos preserves fresh volcanic glass and hence presents an opportunity to evaluate spatial variation of elements and isotopic systems most susceptible to mobilisation during alteration.

The chemical characteristics of Troodos are those of supra-subduction zone magmatism rather than a mid-ocean ridge (Pearce et al., 1984; Rautenschlein et al., 1985). Enrichment of the fluid-mobile elements (Pb, Ba, Rb, Cs, K) and a high water content are indicative of a contribution from fluids leaving the subducting slab (Konig et al., 2010; Woelki et al., 2020). This enrichment develops Ba/La and Ce/Pb which deviate significantly from typical mantle values (Woelki et al., 2018). For example, Ba/La in mid-ocean ridge basalt (MORB) is 2–6 but in Troodos is in the range 10–120, which is more typical of island arc magmas. Given the arc-like chemistry, it is postulated that Troodos developed at a spreading centre in an arc or fore-arc setting (Taylor et al., 1992), similar to the trench-proximal environments found in the northern Tonga arc or trench (Cooper et al., 2010; Falloon et al., 2008), Andaman Sea (Moores et al., 1984) or in the fore-arc at the initiation of subduction (Ishizuka et al., 2014).

* Corresponding author.
E-mail address: rex@soton.ac.uk (R.N. Taylor).

https://doi.org/10.1016/j.epsl.2022.117509

Volcanics in the Troodos ophiolite span a range of compositions from 53–56 wt% SiO_2 at 9–13 wt% MgO ~ 13 wt% MgO at 53.5 wt% SiO_2 through to more differentiated lavas with 7% to <2% MgO (Pearce and Robinson, 2010; Shen et al., 2020). Troodos lavas are predominantly boninite series volcanics, specifically low-silica boninites in the classification scheme of Pearce and Reagan (2019), with some higher-Ti samples falling into the siliceous high-Mg basalt category. The Low-silica boninites and Si-Hi-Mg basalts are olivine ± clinopyroxene ± orthopyroxene phyric, with plagioclase present in the groundmass of lower-Mg lavas (<8%). Differentiated samples are plagioclase-pyroxene phyric high-Mg andesites, andesites and dacites, and are generally found in the lower part of the volcanic sequence. These were referred to as the Lower Pillow Lavas by early geological mapping surveys (Bear, 1960; Gass, 1960) and contrasted with the more primitive, high-Mg, olivine-phyric Upper Pillow Lavas (Cameron, 1985; Rautenschlein et al., 1985; Thy et al., 1985). Such a two-layer stratigraphy is certainly an oversimplification, with primitive and evolved lavas juxtapositioned in some stratigraphic sections (Taylor, 1990; Thy and Esbensen, 1993).

Troodos lavas testify to a mantle source that was depleted relative to a typical MORB source. This depletion is variable, with the boninite and Si-Hi-Mg basalts having TiO_2 ranging from 0.2–0.7 wt% and Zr from 4–40 ppm, all at around 8–10 wt% MgO. Rare earth elements (REE) also reflect these characteristics in their variable depletion of middle relative to heavy REE, with $Dy/Yb_{(n)}$ 0.66–1.0 (Taylor and Nesbitt, 1988; Coogan et al., 2003).

Isotopically, Troodos has the high radiogenic Sr isotope characteristics of island arc magmas, but also has a diverse range of Nd and Pb isotope ratios, indicative of mixing between subducted crust and MORB-like mantle or mantle melts (Cameron, 1985; Konig et al., 2008). Strong evidence for the involvement of sediments in the generation of these magmas comes from B isotopes and the high $^{207}Pb/^{204}Pb$ (Fonseca et al., 2017; Woelki et al., 2018). However, the stratigraphic, spatial and, by association, temporal variation in radiogenic isotopes across Troodos is relatively unexplored.

In this paper, we present high-resolution double spike Pb isotopes with associated major element, trace element and Sr-Nd radiogenic isotope data for 60 samples of fresh volcanic material from across Troodos. These data, with sample locations are provided in Supplementary Data Table S1. We use this information to investigate the influence of slab and mantle on the elemental make-up of subduction volcanism. However, what also emerges is a novel view of the tectonic and geochemical relationships around this Cretaceous intra-oceanic destructive plate margin. In particular, we utilise the spatial geochemistry to clarify: the spreading history and structure of the ophiolitic crust; the relationship between the tectonic and lithological units on the subducting slab and overriding plate; the position of Troodos with respect to global isotopic heterogeneities in the mantle.

2. Samples and methodology

2.1. Nature and distribution of volcanic samples

The vast majority of volcanic rocks found across the Troodos ophiolite experienced some degree of hydrothermal alteration to zeolite facies soon after their formation at a spreading centre. However, despite its Cretaceous age, many volcanic units contain relatively fresh glass as rinds to pillows or at the margins of massive flows. These glasses are present in all of the lithologies represented through the volcanic stratigraphy, and across most areas of the extrusive sequence. The volcanic glass varies from pristine shards attached to pillow rinds, to orbicules and spall found in hyaloclastite, pillow rim zones and around massive flows. To enable geographical coverage all types of glass were sampled in this study, with efforts made to exclude alteration in the form of clays or bleaching.

Glassy rims were segregated and ultrasonically pre-cleaned in pure water, and selected fragments of this material were used for the analyses. This whole-sample methodology was preferred to picking of glass-only shards as it was more likely to integrate any isotopic heterogeneity that may be present in samples as documented by Fonseca et al. (2017). Loss on ignition for whole glass samples is typically 2.5–4.5%, with higher values in other samples suggesting some degree of glass hydration. Analyses were screened to check for samples with anomalous $^{238}U/^{204}Pb$ (>9 or <2), particularly those with >0.5wt% K_2O which would indicate significant element loss or addition. Pb and Sr isotope data was collected on strongly leached microscopically-selected glass chips and is detailed in section 2.2. Samples taken from the same eruptive units in the Margi area (supplementary Table S1) demonstrate that Pb isotope ratios are within double spike error both before and after age correction, this is despite differences in loss on ignition and glass appearance.

Sampling the fresh lavas to constrain isotopic evolution has the potential to be biased by a slightly greater abundance of unaltered material in the upper primitive lavas, and therefore not recognising stratigraphic isotope changes. To reinforce the coverage, and integrate the Pb isotope signal from the bulk of the volcanic sequence, we have incorporated data from Fe-Cu sulphide ore deposits. These are the products of leaching metals from the pre-existing lava sequence and the underlying sheeted dykes. Data sources and Pb isotope uncertainties for ore deposit material is detailed further in section 2.3 below. It should be noted that all azimuthal references in this study; North, West etc., refer to present-day coordinates, rather than the orientations at 91 Ma, prior to the ~90° anticlockwise rotation of the Troodos crust.

2.2. Analytical methods

Rocks were prepared by crushing inside a plastic envelope using a non-torque press. Crushed material was then separated to 0.5–1.0 mm chips using a Teflon sieve set, and then repeatedly cleaned with ultra-pure water in an ultra-sonic bath. Cleaned rock-chips were then purified during a microscopic examination.

Major elements were analysed by X-ray fluorescence (XRF) by fusion of a mixture of subsamples of 0.5 g and lithium tetraborate in a ratio of 1:10. Analysis was using Philips Magix Pro WD-XRF in the School of Ocean and Earth Science, University of Southampton, UK or an equivalent instrument in the Geological Survey of Japan. Error and external accuracy was generally <2% for all samples. REE, Rb, Sr, Y, Zr, Nb, Cs, Ba, Hf, Pb, Th and U concentrations were determined by ICP-MS at SOES on a VG Plasmaquad PQ2+ instrument. Reproducibility is better than ±4% (RSD.) for the REE, Rb and Nb, and better than ±6% (RSD) for other elements. The precision of the elemental ratios is better than ±1% (RSD).

Around 0.3 g of each rock was picked from the 0.5–1.0 mm fraction for isotopic analysis. All samples were leached for 30–40 min in 4M HCl at 200 °C in a sealed Teflon vessel prior to Pb separation using HBr-HCl anion exchange columns. Pb isotope ratios were measured by a Thermo Neptune MC-ICP-MS in the School of Ocean and Earth Science, University of Southampton UK, using a double spike run of each sample to correct for instrumental mass fractionation. The ^{207}Pb–^{204}Pb SBL74 spike (Taylor et al., 2015) was added such that $^{204}Pb_{sample}/^{204}Pb_{spike}$ was 0.09 ± 0.03. Procedural blanks range between 30–105 pg Pb. NBS SRM 981 values achieved during the measurement period were $^{206}Pb/^{204}Pb = 16.9404 \pm 24$, $^{207}Pb/^{204}Pb = 15.4969 \pm 26$, $^{208}Pb/^{204}Pb = 36.7169 \pm 66$ (2sd; n = 44).

For Sr analysis, the Pb residue was evaporated and dissolved in 3M HNO_3. The Sr was isolated using Sr resin (Eichrom Industries,

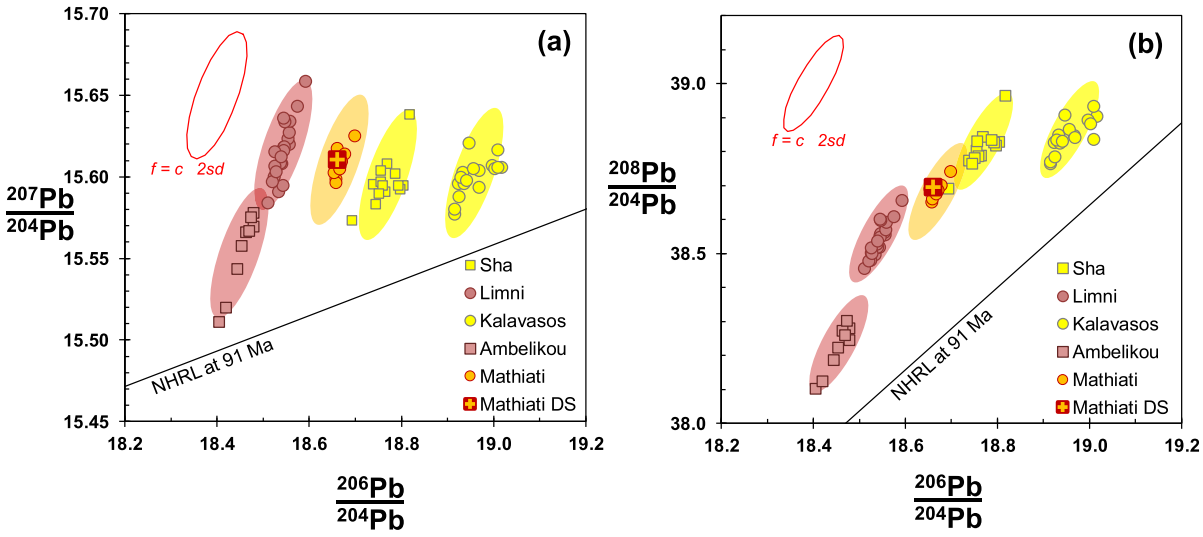

Fig. 1. (a) $^{206}Pb/^{204}Pb$ vs $^{207}Pb/^{204}Pb$ and (b) $^{206}Pb/^{204}Pb$ vs $^{208}Pb/^{204}Pb$ for selected ore deposits from the Oxalid database. Uncertainty ellipses are calculated as 2sd for $f = c$ correction after Taylor et al. (2015) and are centred on the average value for each mine. Mathiati DS is a double spike analysis of a pyrite from this from this study. Northern hemisphere reference line (NHRL; after Hart (1984)) corrected back to 91 Ma (NHRL at 91 Ma). All ore deposit data on this plot are not age corrected.

Illinois, USA). For Nd isotopic analysis, the REE were initially separated by cation exchange, before isolating Nd on Ln resin (Eichrom Industries, Illinois, USA) columns. Sr and Nd isotope ratios were measured on a nine-collector VG Sector 54 mass spectrometer at the Geological Survey of Japan, or on a similar instrument at the University of Southampton, as the average of 150 ratios. Reported values are the average of 150 ratios obtained by measuring ion intensities in multidynamic collection mode normalised to $^{86}Sr/^{88}Sr = 0.1194$ and $^{146}Nd/^{144}Nd = 0.7219$. Measured values for NBS SRM-987 and JNdi-1 were $^{87}Sr/^{86}Sr = 0.710237 \pm 15$ (2 SD, n = 58) and $^{143}Nd/^{144}Nd = 0.512104 \pm 7$ (2 SD, n = 64) on both instruments during the measurement period. The Sr and Nd isotopic data presented here have been normalised to NBS SRM-987 (0.710248) and JNdi (0.512110).

2.3. Ore deposit Pb isotope data

Fresh lava and volcanic glass is not available in all geographic locations or stratigraphic positions around the Troodos ophiolite. Therefore, to increase spatial isotopic coverage, we have utilised the "Oxalid" Pb isotope database (Gale et al., 1997; Stos-Gale and Gale, 2009), which includes sulphide mineral isotope data from all hydrothermal deposits across Cyprus. These data were collected using a constant−f mass fractionation correction ($f = c$) using traditional thermal ionisation mass spectrometry in the 1980s and 1990s, and hence contains an inherent measurement uncertainty that is 10–15 times larger than the double spike data presented in this study (Taylor et al., 2015). Beneficially though, the high Pb concentrations of the ore minerals (10–1000 ppm) mean that these measurements are less prone to the effects of blank contamination and are hence likely to be accurate, if imprecise.

To enhance the precision of the ore data and enable comparison with our high-precision lava analyses, we have used the average isotopic compositions of each deposit. If it is assumed that ores from each mine are isotopically homogeneous, and that any scatter in Pb isotopes is generated by measurement uncertainty, then Pb isotope ratios for each mine should be normally distributed about their mean. As such, the effect of averaging will more tightly constrain the true value in proportion to the number of samples, with uncertainty expressed as $2\sigma/\sqrt{n}$ at 95% confidence. The effects of this averaging technique are tested in Fig. 1, which shows that data from representative mines are distributed within the bounds of the appropriate $f = c$ uncertainty ellipse for the given ratio pairs. An ore sample from Mathiati mine was measured in this study by double spiking, and lies at the centre of the non-double spike data from the same mine (Fig. 1) and is within double spike uncertainty of the non-double spike average. All ore data is compiled and presented with location information and statistical analysis in Supplementary Data Table S2. An interesting feature of the uncertainty ellipse in $^{206}Pb/^{204}Pb$–$^{207}Pb/^{204}Pb$ (Fig. 1a) is that it is roughly parallel to lines of constant $^{207}Pb/^{206}Pb$. This reduces the likelihood of analytical deviation from the true $^{207}Pb/^{206}Pb$ in $f = c$ corrected Pb data such as the Oxalid database.

Pb is more compatible with pyrite and chalcopyrite than U and Th, and consequently hydrothermal sulphide deposits typically have low μ-values ($^{238}U/^{204}Pb$). Mid-ocean ridge pyrites have $\mu \sim 0.5 \pm 0.4$ (Wang et al., 2018), which is more than 20 times lower than typical MORB lavas. A pyrite ore we have measured from the Mathiati mine has $\mu = 0.4$ and ω ($^{232}Th/^{204}Pb$) = 0.0042 which are 14 and 3000 times lower respectively than the averages for Troodos lavas. This means that the 91 Ma age-correction of Pb isotopes for Cyprus sulphides is essentially negligible, with $^{206}Pb/^{204}Pb$ in the Mathiati pyrite decreasing by 0.0057. On this basis, and as U-Th-Pb concentrations are not available for the Cyprus ore database, Pb isotopes for the sulphide minerals are presented as averages of the measured values are alongside the age-corrected ratios for the Troodos lavas. Ore Pb isotope data is only used to help constrain spatial variation, and is excluded from the assessment of geochemical dynamics in the Troodos subduction system, where only the high-precision double spike data is used.

2.4. Constraining spatial isotopic variation

An objective of this study is to examine the spatial variation of isotopes and trace element characteristics across the Troodos ophiolite. Here, rather than split the ophiolite into geographical regions and look for contrasting geochemistry, our method is to identify particular geochemical parameters of interest and examine how they are disposed spatially. Of the radiogenic isotope systems, Sr isotopes have the potential to be dominated by a seawater or radiogenic compositions in all subducted materials, and are the most susceptible to modification during hydrothermal circulation. Because Pb has relatively low concentrations in seawater, it is a more robust isotope system with which to discriminate subduction components involved in Troodos magma genesis. In addition, a feature of the Pb isotope ratios is the wide range of values present across

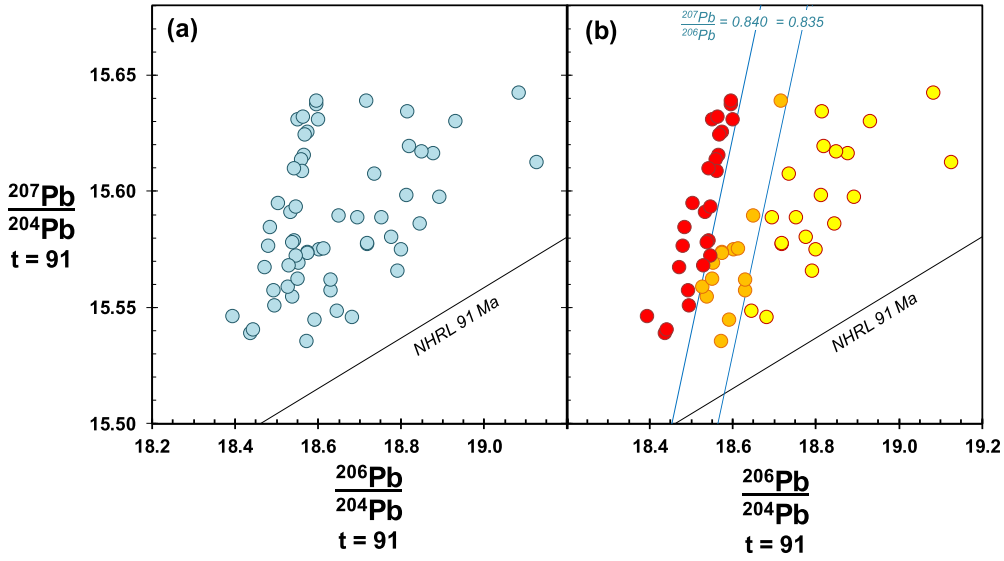

Fig. 2. $^{206}Pb/^{204}Pb$ vs at $^{207}Pb/^{204}Pb$ for Troodos volcanics. (a) Data undifferentiated; (b) data coded according to $^{207}Pb/^{206}Pb$. All data are age corrected to 91 Ma. (For interpretation of the colours in the figure(s), the reader is referred to the web version of this article.)

the ophiolite: $^{206}Pb/^{204}Pb$ spanning 18.4 to 19.1 (Fig. 2). This range is ∼200 times greater than our Pb measurement precision, meaning that it has a higher resolving power compared to $^{143}Nd/^{144}Nd$, which has a range/precision of around 40.

The undifferentiated $^{206}Pb/^{204}Pb$–$^{207}Pb/^{204}Pb$ data in Fig. 2a broadly define two sub-aligned clusters of samples: a group with $^{206}Pb/^{204}Pb \sim 18.5$ with a steep positive trend, and a dispersed group with a shallower positive correlation extending to $^{206}Pb/^{204}Pb \sim 19.1$. The steep positive trend lies roughly along a line with equal $^{207}Pb/^{206}Pb$ (∼0.842 at 91 Ma) and the shallower tend has $^{207}Pb/^{206}Pb < 0.839$. On this basis we have chosen to differentiate the samples based on their $^{207}Pb/^{206}Pb$. Fig. 2b shows the samples coded as red with $^{207}Pb/^{206}Pb > 0.840$, orange with $^{207}Pb/^{206}Pb$ 0.840–0.835 and yellow with $^{207}Pb/^{206}Pb < 0.835$. This division of samples and their associated colours are retained through subsequent geochemical and geographic figures. Based on isotopic characteristics, we refer to the low $^{207}Pb/^{206}Pb$, high $^{206}Pb/^{204}Pb$ group as HiMu (Zindler and Hart, 1986): HiMu (or high-μ) refers to high $^{238}U/^{204}Pb$ in material that has generated, or has the potential to generate, high $^{206}Pb/^{204}Pb$.

3. Tectonic and isotopic systematics of the ophiolite

A lithological and structural summary of the Troodos ophiolite is provided in Fig. 3a, and a matching map showing the distribution of the $^{207}Pb/^{206}Pb$ divisions is shown in Fig. 3b.

Measured strike of dykes varies across the ophiolite. In the west of Troodos dykes are dominantly N-S or NW-SE, but from Troodos village eastwards they progressively realign to NE-SW (Fig. 3a). Further east towards Larnaca the dykes revert to NW-SE. Although these dyke orientations can be a guide to spreading direction, they can be significantly affected by post-intrusion block rotation about vertical and horizontal axes. Restoration of palaeomagnetic measurements of dykes to a reference declination and inclination gives a more accurate picture of the spreading axis alignment (Allerton and Vine, 1987; Morris et al., 1990). After restoration to initial dyke orientations across the ophiolite (Fig. 3a) it is apparent that spreading axis orientation was NW-SE (Abelson et al., 2002; Allerton and Vine, 1991; Maffione et al., 2017; Morris and Maffione, 2016; Scott et al., 2013). The most significant rotation of dykes is observed north of the exposed section of the Southern Troodos Transform Fault (Fig. 3a). This dyke re-orientation is taken to represent a clockwise rotation of blocks related to dextral slip along this section of the transform (Cooke et al., 2014; MacLeod et al., 1990; Morris et al., 1990). Limited rotation to the east and west of the exposed transform could reflect no slip or limited slip along these sections due to crust either side of the fault moving in the same direction at a similar rate (Allerton, 1989; Allerton and Vine, 1991). These kinematics are consistent with the position of the Solea axis e.g. Moores et al. (1990); Varga and Moores (1985) and a concurrent axis located south of the transform and east of the ophiolite (Abelson et al., 2002; van Everdingen, 1995).

Overall, the Pb isotope variation across Troodos shows that the east and south east of the ophiolite has the low $^{207}Pb/^{206}Pb$ HiMu signature (Fig. 3b). Specific spatial observations are: 1) The HiMu signal increases eastwards across the north eastern flank of the ophiolite, 2) in the east the HiMu signal extends from the northern to the southern margin of the ophiolite and is not exclusive to the transform domain, 3) HiMu is present across the crust south of the transform, but non-HiMu is also present at the western end of this crust, 4) samples at each location across the ophiolite have similar characteristics, regardless of position within the stratigraphy or whether of lava or mineralisation.

The easterly progression to HiMu is interesting because it is not symmetrical across the north of the ophiolite. This is inconsistent with simple spreading about a single axis, located near the centre of Troodos (such as the Solea axis, Fig. 3a) as it would be expected that HiMu would be present in the westernmost exposures to mirror those in the east. It is however possible that the crust north of the transform could have developed at a long-lived spreading axis located west of current Cyprus, as proposed by Mackenzie et al. (2006). Alternatively, the crust could have been generated by an eastward jump of the spreading axis (Moores et al., 1990). In this case, the youngest crust would lie to the east, generated following a shift in spreading from the Solea axis to Larnaca axis, moving the active volcanism into the zone of HiMu influence.

The exact position of the boundary between the hypothesised Solea and Larnaca spreading domains is not well defined. Allerton and Vine (1991) located the boundary to the east; whereas other studies (Martin et al., 2019; Moores et al., 1990) positioned it further west (the eastern and western dotted lines respectively in Fig. 3a). Comparing Figs. 3a and 3b it is observed that the eastward onset of the HiMu influence is coincident with the westerly boundary, whereas it straddles the easterly boundary. In the case of the easterly boundary, the oldest crust generated at the Solea

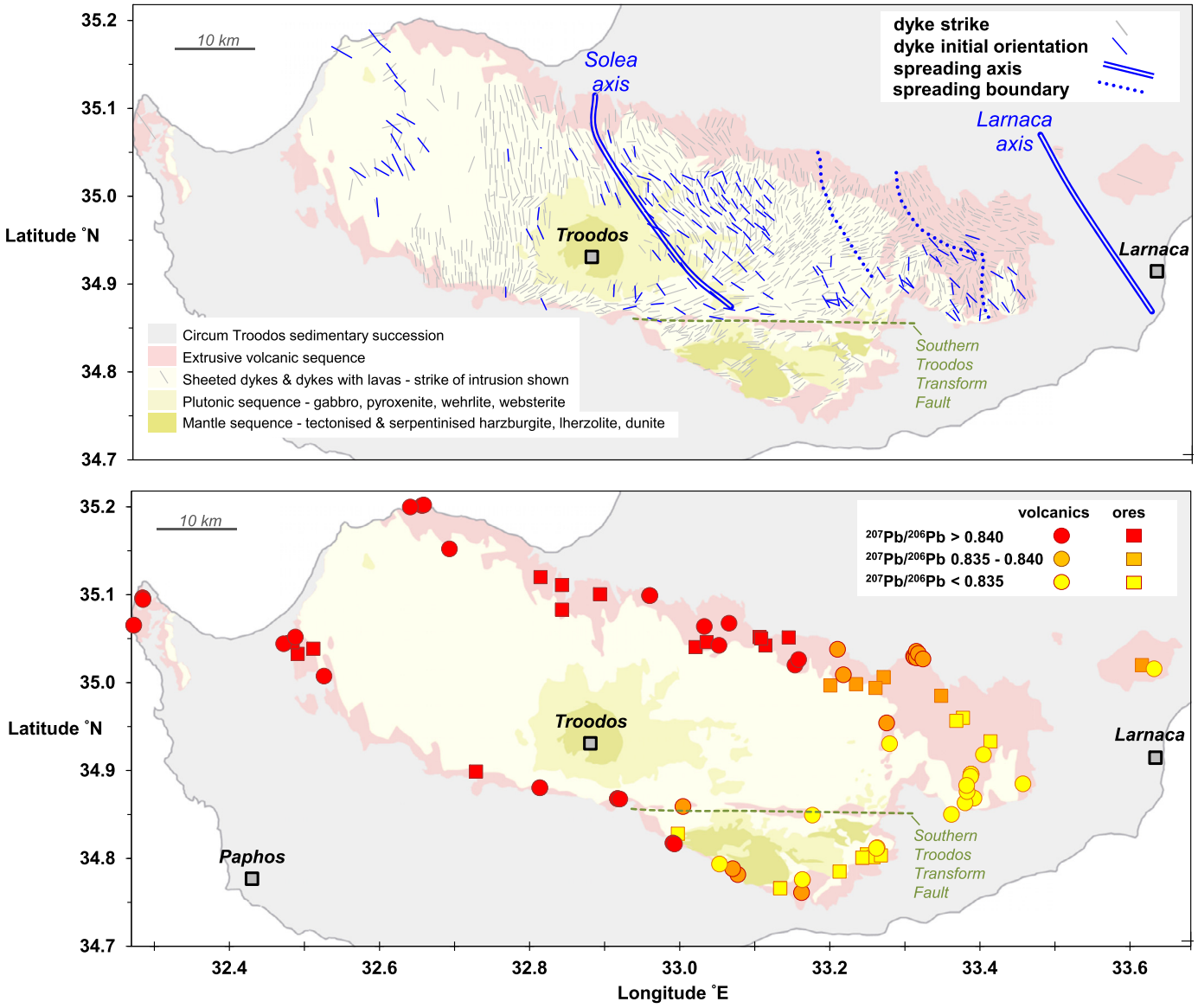

Fig. 3. Geological map of the Troodos ophiolite – adapted from Geological Survey of Cyprus geological maps and memoirs. (a) Key structural features: observed dyke strikes; dykes rotated to initial orientations restored via direction in which they acquired their magnetisation; postulated spreading axes; boundaries between axial spreading domains; Southern Troodos Transform Fault. Initial dyke orientations from (Abelson et al., 2002; Allerton and Vine, 1991; Cooke et al., 2014; MacLeod et al., 1990; Maffione et al., 2017; Morris et al., 1990; Morris and Maffione, 2016; Scott et al., 2013). (b) Sample locations for volcanics and ores coded according to $^{207}Pb/^{206}Pb_{t=91}$.

axis would have been located in the HiMu zone. Subsequently, the Solea axis may then have migrated westwards away from the HiMu influence. However, what is missing from this arrangement is any evidence for a symmetrical HiMu signature in the far west of the ophiolite. In the case of the westerly boundary, Solea spreading would have been exclusively in the non-HiMu region, and a ridge jump to the Larnaca axis initiating spreading in the HiMu zone.

As the HiMu influence is found across the crust south of the transform it is possible that this material was generated at a spreading axis to the east: just south of Larnaca in Fig. 3a. Westward spreading from this axis displaced this crust relative to the material north of the transform via the expected dextral slip and sinistral ridge-offset.

As noted above, the western end of the crust south of the transform appears to have both HiMu and non-HiMu characteristics in close proximity. The sample with the HiMu signature in this location is from a Cu sulphide ore, which is likely to have integrated the signal from the lower sections of the lavas and dykes, while the non-HiMu samples are from the boninitic upper lavas. This could be the result of a superimposition of later non-HiMu volcanism on pre-existing HiMu crust. Lavas with a similar non-HiMu composition are also found just north of the transform, and it is therefore possible that these late-stage lavas represent the waning, youngest volcanic activity of the Solea axis, and were fed via late NW-SE boninitic dykes (Gass et al., 1994) propagating southwards across the transform. This needs to be tested by a more extensive isotopic characterisation of crustal units in this region. However, in most other areas of the ophiolite the ore deposits have Pb isotopes that match the local lavas, indicating that the high, intermediate and low-$^{207}Pb/^{206}Pb$ signatures are characteristic of the whole crustal section at a given location.

Geochemical parameters other than Pb isotopes have been identified as varying systematically across Troodos. In particular, incompatible elements are recognised as having progressively lower concentrations relative to moderately incompatible elements (e.g. TiO_2/Al_2O_3, MREE/HREE) towards the south of the ophiolite (Taylor and Nesbitt, 1988); taken to mark a southward progression to a more depleted and shallower mantle source located closer to

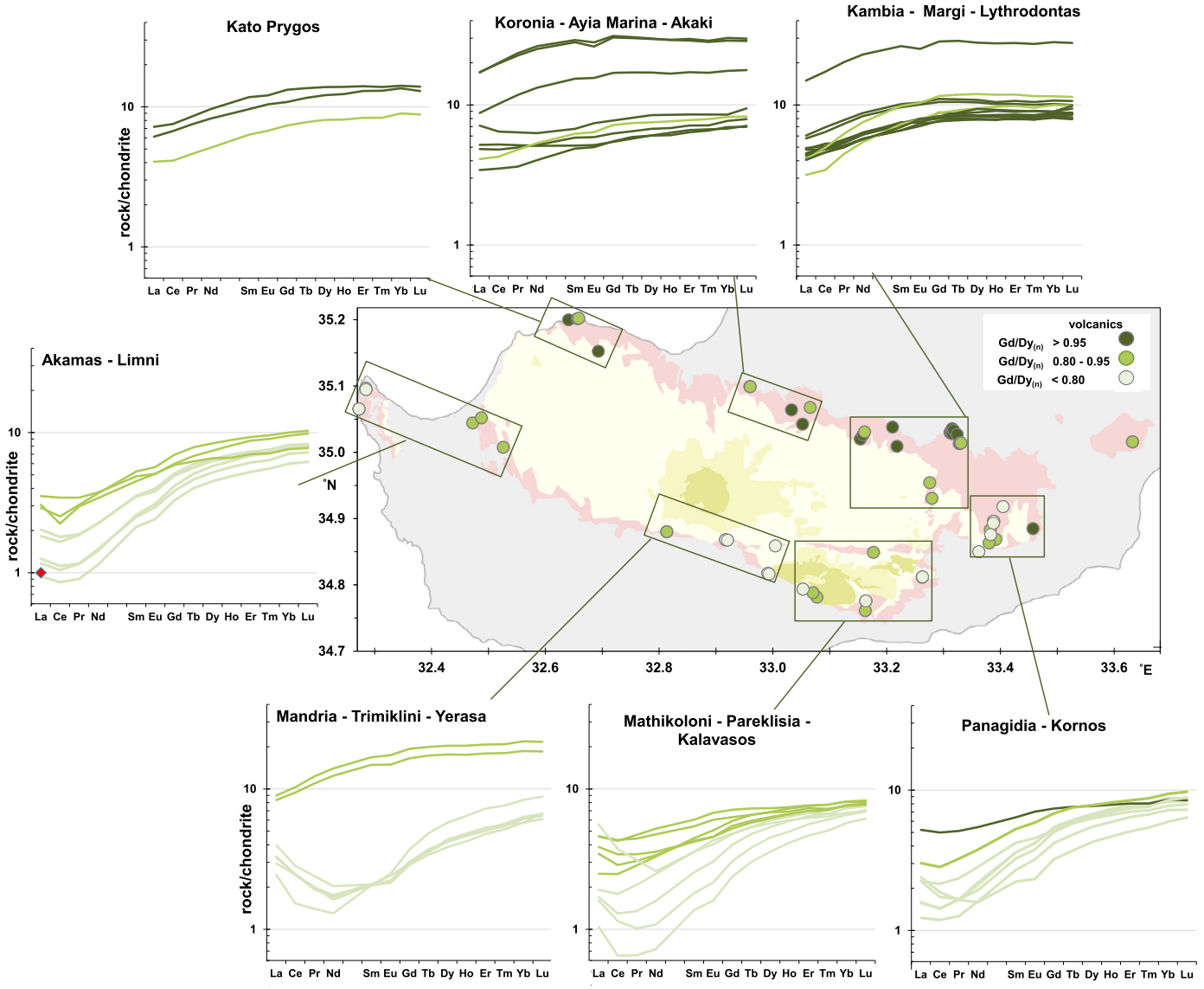

Fig. 4. Chondrite normalised rare earth element patterns from across the Troodos ophiolite. Samples are colour coded according to $Gd/Dy_{(n)}$. Elemental and location data is given in Table S1.

the trench (Taylor et al., 1992). These spatial characteristics are shared with modern arc environments (Escrig et al., 2012; Taylor et al., 1992; Woelki et al., 2019). Fig. 4 shows that northern Troodos has moderately depleted LREE and chondritic $Gd/Dy_{(n)}$ (>0.95), whereas southern Troodos has these compositions alongside highly LREE depleted lavas with $Gd/Dy_{(n)} < 0.8$. This tendency for greater LREE depletion from north to south (Fig. 4) is effectively independent of the variation in Pb isotopes (Fig. 3b) which show a transition to HiMu from west to east.

4. Sources of isotopic variation

To examine the causes of the Pb isotope variation, we first set out the potential inputs that could have influenced the Pb isotopic composition of the Troodos spreading system. These are: the subducted slab, comprising sediments, igneous ocean crust and volcanic seamounts; and the mantle wedge, potentially of a MORB or OIB-like character. Given the spreading nature and extent of the Troodos crust, effects of lithospheric assimilation are likely to be limited. Compositions of these key components are highlighted in Fig. 5 and detailed below. Using this component framework, we then discuss the interaction between subducted components and the mantle wedge.

Fig. 5 uses three different Pb isotope projections: $^{206}Pb/^{204}Pb$–$\Delta^{207}Pb$, $^{206}Pb/^{204}Pb$–$\Delta^{208}Pb$, and $\Delta^{207}Pb$–$\Delta^{208}Pb$, which are shown in Fig. 5a-5b, 5c-5d, and 5e respectively. $\Delta^{207}Pb$ and $\Delta^{208}Pb$ are vertical deviations of a sample's $^{207}Pb/^{204}Pb$ and $^{208}Pb/^{204}Pb$ respectively from the NHRL expressed in units of the second decimal place of their ratio: as defined by Hart (1984). Sample groupings (based on $^{207}Pb/^{206}Pb$) show similar dispositions in $\Delta^{207}Pb$ and $\Delta^{208}Pb$ (Fig. 5a and 5c), with the non-HiMu group (red) forming a steep trajectory from low to high ΔPb, and the HiMu group (yellow) forming broad positive correlations from low to high $^{206}Pb/^{204}Pb$ (~18.6-~19.1).

4.1. Sediments

Subducted sediment compositions in the Cretaceous are best represented by deposits in the current Eastern Mediterranean, which overlie remnants of Jurassic-Triassic Tethyan ocean crust (Klaver et al., 2015) and are likely to have a similar provenance. An average of these sediments currently has $^{206}Pb/^{204}Pb \sim 18.9$,

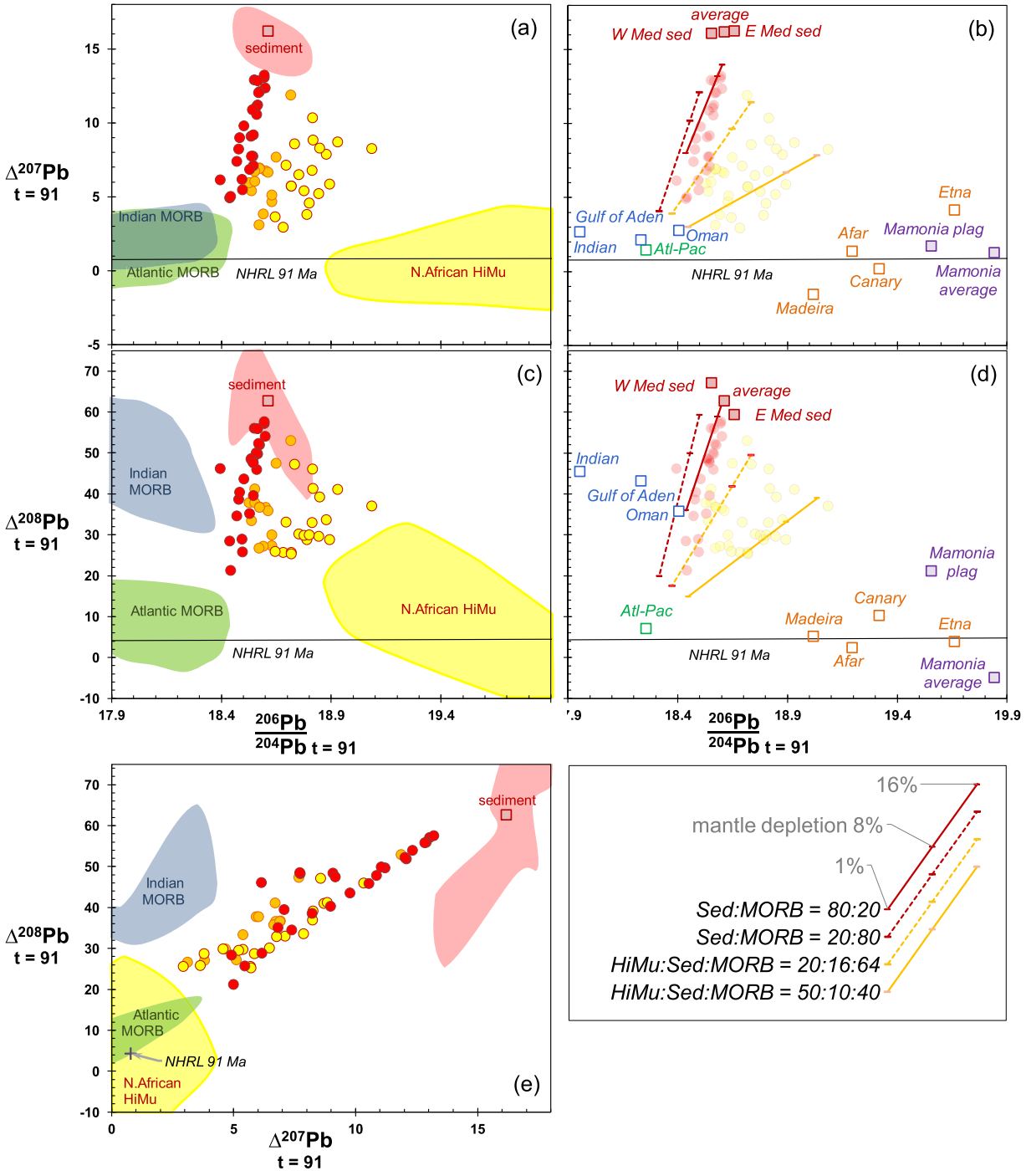

Fig. 5. Pb isotopes of Troodos volcanics categorised by $^{207}Pb/^{206}Pb_{t=91}$. Colour coding as for Fig. 2. (a & b) $^{206}Pb/^{204}Pb$–$\Delta^{207}Pb$, (c & d) $^{206}Pb/^{204}Pb$–$\Delta^{208}Pb$, (e) $\Delta^{207}Pb$–$\Delta^{208}Pb$. (a, c & e) Show fields for: Atlantic MORB and Indian MORB containing >75% of data from Tl-spike or double spike analyses compiled after Meyzen et al. (2007); Mediterranean sediments analysed via double spike (Klaver et al., 2015; Rodrigo-Gamiz et al., 2015); North African HiMu plumes. (b & d) Show average values for: Atlantic/Pacific MORB & Indian MORB compiled after Meyzen et al. (2007); Oman Triassic MORB (Lapierre et al., 2004); Gulf of Aden (Schilling et al., 1992); Madeira (Geldmacher and Hoernle, 2000; Geldmacher et al., 2006), Afar (Deniel et al., 1994; Rooney et al., 2012), Canary (Taylor et al., 2020), Etna (Nuccio et al., 2008); enriched Mamonia volcanics (Lapierre et al., 2007); Mamonia plagioclase separate (this study). Component isotope data listed in Supplementary data Table S1. (b & d) Show modelled trajectories for melting of variably-depleted mantle, metasomatised with four different hybrid fluids –further details of the modelling in the text.

$\Delta^{207}Pb \sim 15$ and $\Delta^{208}Pb \sim 50$ (18.66, 16.3 and 60 respectively at t = 91 Ma). Sediments of this composition have the potential to be a high $\Delta^{207}Pb$ and $\Delta^{208}Pb$ subduction component, particularly given the similarity between the Pb isotope ratios of the Aegean arc (Klaver et al., 2016) and the Troodos ophiolite. $^{87}Sr/^{86}Sr$ of Mediterranean sediments is 0.708–0.717 at 91 Ma, and hence could generate the high and variable ratios of the Troodos lavas.

4.2. Igneous ocean crust

Constraints on the nature and composition of the subducting igneous crust can be gained from ophiolites along the length of the Tethyan suture. Some are thought to represent obducted Neo-Tethyan spreading centre crust, or remnants of back-arc or marginal basins. Generally these ophiolites have $^{206}Pb/^{204}Pb$ 18.0–18.5 (Chauvet et al., 2011) and have N-MORB characteris-

tics. It has been hypothesised based on Pb–Nd isotopes that such ophiolites indicate the Tethys ocean crust was generated from what today is the Indian Ocean mantle domain (Mahoney et al., 1998; Zhang et al., 2005). Triassic MORB-like lavas found adjacent to Oman (Lapierre et al., 2004) could represent stranded Tethyan crust, and have Pb isotope systematics ($^{206}Pb/^{204}Pb \sim 18.4$; $\Delta^{207}Pb \sim 3$; $\Delta^{208}Pb \sim 36$ at t = 91 Ma; Fig. 5b and 5c) that are roughly equivalent to Indian MORB at that time. Such compositions are also similar to Indian MORB in the Gulf of Aden (Schilling et al., 1992) away from the influence of the Afar plume (Fig. 5b and 5c). Atlantic-type MORB crust could also have been involved in the Troodos system, with Southern European ophiolites (e.g. Albania) suggestive of North Atlantic compositions (Zhang et al., 2005). Fields encompassing >80% of Atlantic and Indian MORB (translated to 91 Ma) are shown on Fig. 5a and 5c, and average Atlantic and Indian MORB values are shown on Fig. 5b and 5d. Strontium isotopes of the subducted ocean crust are more difficult to constrain, but are likely to be between original igneous values of $^{87}Sr/^{86}Sr \sim 0.7025–0.7030$ and hydrothermally altered values characterised by the Oman Triassic MORB (0.706 at 91 Ma).

4.3. OIB seamounts

Volcanic seamount chains of ocean island basalt (OIB) composition are common on many tracts of ocean crust (Haase et al., 2019; Koppers et al., 1998). Their influence on subduction-related volcanism is well documented across the western Pacific, and when subducted wholescale, or as volcaniclastic sediments, can significantly influence the composition of arc volcanism (Ishizuka et al., 2006; Pearce et al., 1999; Peate and Pearce, 1998; Timm et al., 2011). Like the sediments and ocean crust, the seamounts are likely to have interacted with hydrothermal systems and consequently can tend towards seawater $^{87}Sr/^{86}Sr$. Evidence for such material is present in the Mamonia Complex and Moni formation to the south of the Troodos ophiolite as blocks and clasts of material thought to have accreted during collision or collected in the trench during subduction (Robertson and Xenophontos, 1993). These include depleted tholeiitic lavas and OIB tholeiitic and alkaline volcanics thought to be Late Triassic in age (~210 Ma) based on Norian-Carnian fauna in associated limestones (Lapierre et al., 2007). Though predominantly hydrothermally altered, a $^{238}U–^{206}Pb$ isochron constructed from the Mamonia OIB samples (Type 3 & 4; Lapierre et al., 2007), gives an age of 204 ± 7 Ma. This indicates the U-Pb systematics have been consistent since eruption and alteration, and enables an estimate of their initial isotope composition (Mamonia average, Fig. 5b and 5d). Fresh plagioclase feldspar separated from a Mamonia lava in this study (Mamonia plag, Fig. 5b and 5d) validates the Pb isotopic composition from the Lapierre et al. (2007) whole rock data. Corrected to 91 Ma this produces a similar high $^{206}Pb/^{204}Pb$ (~19.6) around the NHRL. Overall, the OIB-like Mamonia lavas are isotopically similar HiMu composition to many plume-related volcanics found around northern Africa, such as the Canaries, Madeira, Etna and Afar. Depleted tholeiitic samples found in Mamonia also have a similar HiMu isotopic flavour, but have less radiogenic Pb; redolent of ridge basalts influenced by a HiMu plume (Lapierre et al., 2007).

4.4. Mantle wedge

The full spreading regime represented by the Troodos suprasubduction ophiolite is likely to have sourced the bulk of its magma from decompression melting of the mantle wedge. Compositionally, this mantle is characterised by REE patterns of the lavas which range from significantly depleted, with sub-chondritic levels of Nd and $Gd_n/Dy_n \sim 0.7$ to less depleted and more "normal" MORB-like with 8 times chondrite Nd and $Gd_n/Dy_n \sim 1$. These values are similar to intra-oceanic arc to forearc systems like Izu-Bonin and Tonga (Falloon et al., 2008; Hickey-Vargas et al., 2018; Li et al., 2019), and imply a variable level of depletion or progressive melt extraction from the mantle wedge e.g. Cooper et al. (2010); Tamura et al. (2007). Isotopically, the wedge is likely to have characteristics similar to MORB, with $^{143}Nd/^{144}Nd_{(91\ Ma)}$ ranging up to 0.5130, and potentially could originate from the Indian or Atlantic mantle domains. It is also possible that the mantle wedge contains an OIB-like component, potentially as a metasomatic small melt fraction trapped within the depleted MORB matrix (Kostopoulos and Murton, 1992).

4.5. Fluid fluxing and interaction with depleted mantle

As a whole, Troodos lavas fall in a roughly triangular Pb isotope array bounded by MORB, sediment and HiMu components (Fig. 5). Western Troodos (red symbols; non-HiMu group) form the low $^{206}Pb/^{204}Pb$ side of the triangle, and consequently define a line between MORB and sediment. More specifically, the western group range between low $\Delta^{208}Pb$ Atlantic MORB and sediment, with some samples having $\Delta^{208}Pb$ 20–30 (Fig. 5c). Eastern HiMu lavas extend away from the MORB-sediment trend towards HiMu, but dominantly lie on a broad trend between Atlantic MORB and a point intermediate between sediment and HiMu.

Interaction between potential subduction fluids (or melts) and the mantle wedge have been modelled and the results plotted on Fig. 5b and 5d. In this modelling the sediment, MORB crust (Indian-type) and HiMu OIB slab components are equilibrated with fluids at 6 GPa and 900 °C using the partitioning values of Kessel et al. (2005). Shallower and hotter combinations 4 GPa and 1000 °C produce similar results, but temperatures <900 °C do not reproduce the observed high field strength element mobility. These components are mixed to form a hybrid "cocktail" fluid, which is then equilibrated with variously depleted mantle (1%, 8% and 16% previous melt extraction) of Atlantic-type. Variably depleted mantle is calculated as the residue after aggregate modal fractional melting of depleted MORB mantle (Workman and Hart, 2005) with no melt retention, using distribution coefficients compiled after White (2020). The mantle/fluid volume ratio is estimated as 50 km^3 of mantle wedge equilibrating with 1 km^3 of slab which releases 1% fluid, i.e. 5000:1. Final magmas are calculated as an 8% aggregate fractional melt of this metasomatised mantle.

Sediment-MORB hybrid fluids added to the variably depleted mantle result in linear Pb arrays (Fig. 5b and 5d). Adding fluid with a higher proportion of sediment relative to MORB (80:20 instead of 20:80) contracts the model array towards sediment in accordance with the ~20x more Pb in sediment relative to MORB. When the variably depleted mantle is fluxed with hybrid fluid equilibrated with HiMu OIB as well as sediment and MORB, the modelled trajectories extend from Atlantic MORB mantle to intermediate points between sediment and HiMu OIB; the exact trend dependent on the amount of HiMu OIB in the hybrid fluid.

The relationship between mantle depletion and subduction enrichment is explored further in Fig. 6. Pb isotopes are inferred to track the origins of the subduction fluid, so Fig. 6a, 6b, 6c and 6d show the variations in $^{206}Pb/^{204}Pb$, $\Delta^{207}Pb$, $\Delta^{208}Pb$ and Nb/Zr respectively with $Gd/Dy_{(n)}$ as the index of mantle depletion. Western Troodos samples (red; non-HiMu) show slight increases in $^{206}Pb/^{204}Pb$ and $\Delta^{208}Pb$, and significant increases in $\Delta^{207}Pb$ with lower $Gd/Dy_{(n)}$. Similarly, Eastern Troodos samples (orange & yellow; HiMu) show broad negative correlations between $Gd/Dy_{(n)}$ and Pb isotopes.

The same modelling systematics used for the Pb–Pb isotopes (Fig. 5) are applied to the enrichment-$Gd/Dy_{(n)}$ modelling in Fig. 6. A feature of these models is that they use three levels of mantle depletion: generated by 1%, 8% and 16% prior melt extraction.

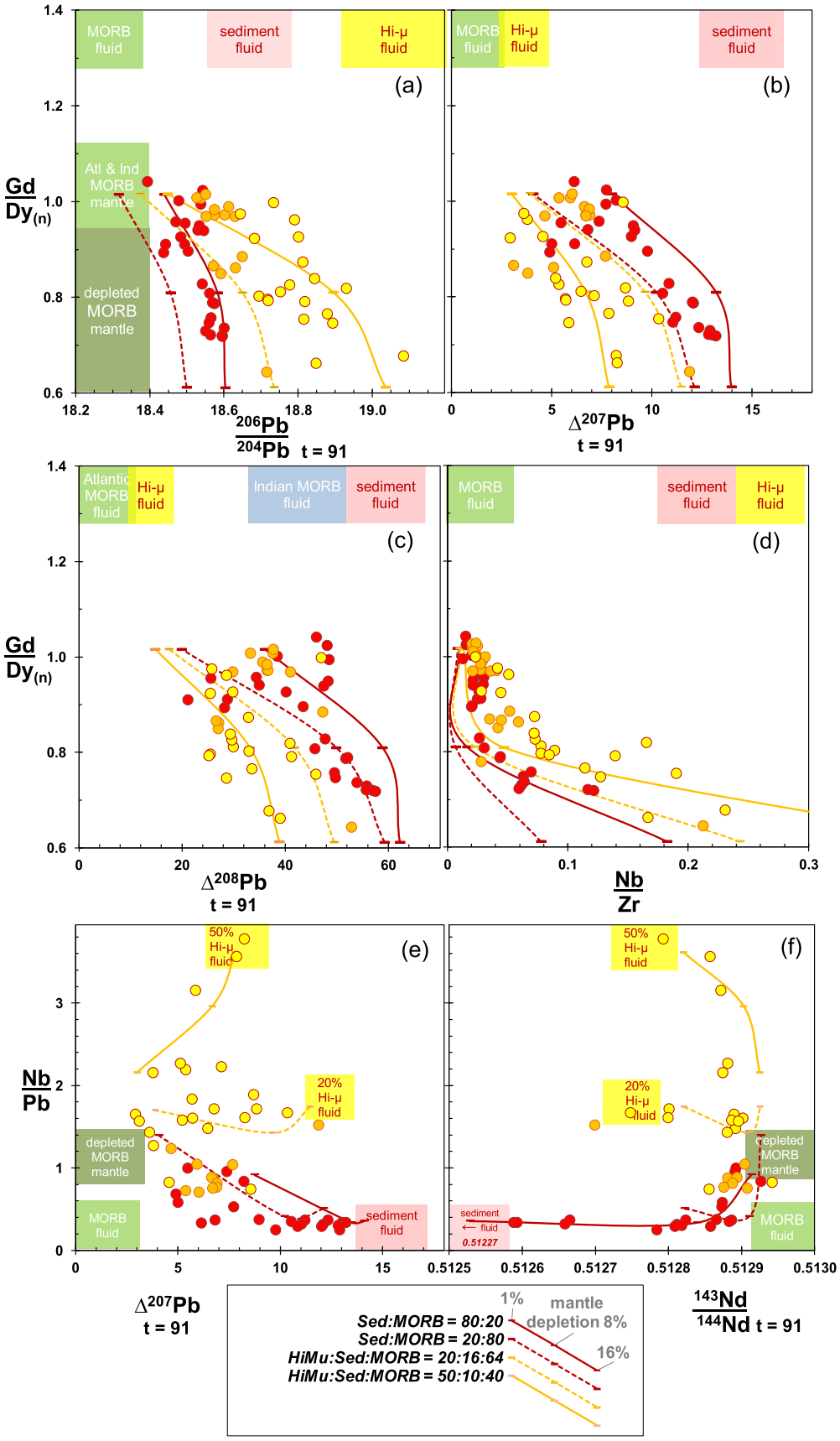

Fig. 6. (a–d) Pb isotopes and Nb/Zr vs $Gd/Dy_{(n)}$ (e & f) $\Delta^{207}Pb$ and $^{143}Nd/^{144}Nd$ vs. Nb/Pb. Colour coding as for Fig. 2; modelling parameters as Fig. 5 and text. Indicative fields for fluid components and the variably depleted mantle wedge are shown.

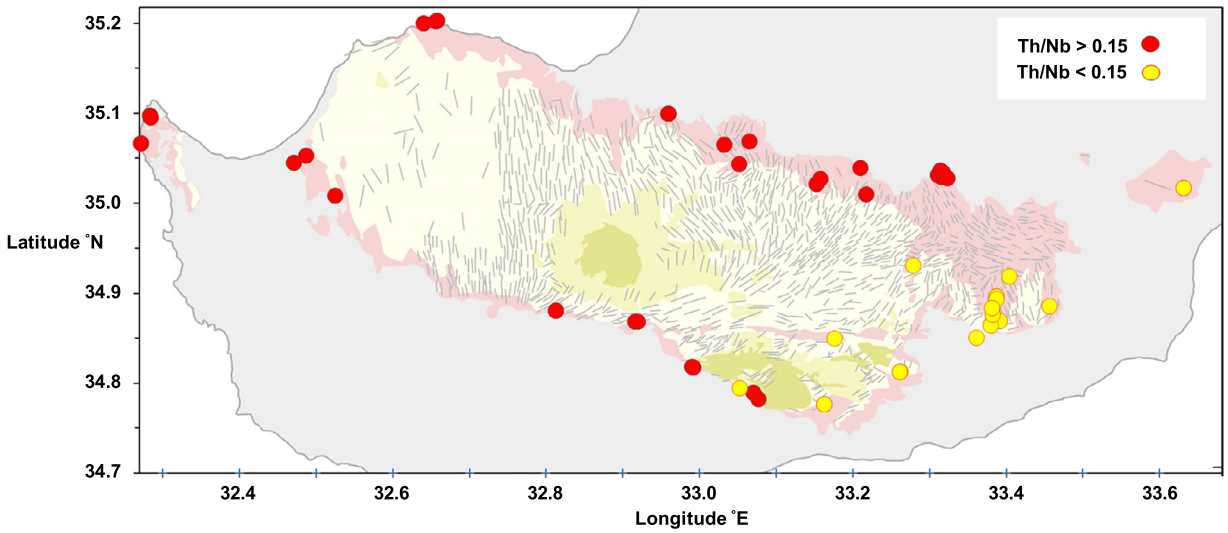

Fig. 7. Distribution of Th/Nb variation across the Troodos ophiolite. Th/Nb partitioned arbitrarily, with ratios <0.15 taken to distinguish high-Nb HiMu lavas.

The 1% depletion having a composition similar to a MORB source, and the 16% equivalent to a highly depleted MORB source with $Gd/Dy_{(n)} \sim 0.6$. So each model in Fig. 6 simulates melting of the three different mantle compositions with a particular hybrid fluid. These models show that melts generated by mantle wedge – hybrid fluid interaction provide a reasonable match for the variations observed in Western and Eastern Troodos.

Compositions of the likely mantle wedge and individual subduction fluid components are also shown on Fig. 6. These fluid components are shown indicatively, as they are likely to have $Gd/Dy_{(n)} > 1.4$. What is clear from the observed sample trends and model trajectories in Fig. 6 is that they do not extend on simple mixing parabola between the MORB mantle wedge and these fluids. Instead, each trajectory appears to represent similar fluid volumes and concentrations added to variably depleted mantle. As the fluid contains essentially no Gd or Dy, these elements are sourced from the mantle wedge, whereas the Pb is predominantly introduced by the fluid. Interestingly, Nb/Zr is also negatively correlated with $Gd/Dy_{(n)}$ (Fig. 6d), and by association correlates positively with $\Delta^{207}Pb$. This suggests that Nb is enriched relative to Zr with the addition of sediment-dominated fluid or melt, but also particularly enriched by the HiMu OIB-rich fluid. Such fluid enrichment of high-field strength elements relative to REE in arcs has been recognised by a number of studies, e.g. Woodhead et al. (2011). Fluids at 6 MPa and 900 °C in equilibrium with OIB have ~28 ppm Nb, whereas the sediment and MORB fluids have 6 and 1 ppm respectively, which is consistent with the particularly high Nb, Nb/Zr and low Th/Nb found in the Eastern Troodos HiMu lavas.

Enrichment of Nb via subduction fluid is explored further in Fig. 6d and 6e. Non-HiMu have a variable Nb/Pb in the lavas with lower $\Delta^{207}Pb$ (<~8) and higher $^{143}Nd/^{144}Nd$ (>0.51287), but have consistent Nb/Pb as $\Delta^{207}Pb$ increases and $^{143}Nd/^{144}Nd$ decreases. This indicates that increasing input of sediment-dominated fluid results in a synchronous and proportional enrichment in Nb, Pb and Nd. In contrast, the HiMu eastern lavas show consistent or increasing Nb/Pb with increasing $\Delta^{207}Pb$ and slightly decreasing $^{143}Nd/^{144}Nd$. An implication is that increased addition of their hybrid fluid produces a greater enrichment in Nb, which is in line with the mixing models involving variable proportions of HiMu in the hybrid fluid. Greater enrichment of Nb in the HiMu-influenced lavas is observed to match the spatial variation of HiMu Pb isotopes. Fig. 7 shows the variation in Th/Nb across Troodos, with low ratios dominating the south east and south of the ophiolite. This parameter lacks the finesse of the Pb isotopic discrimination, however, it does show that low Th/Nb is present in both highly depleted and less depleted samples (e.g. Fig. 4) across eastern Troodos.

A key feature we observe in the Troodos lavas is the negative correlation between $Gd/Dy_{(n)}$ and Pb isotopes (Fig. 6a-c). It is possible that adding more fluid would increase the degree of melting and hence lower $Gd/Dy_{(n)}$ (Taylor and Nesbitt, 1988), but this is not consistent with the fact that Pb and other fluid mobile elements have similar abundances in samples with low and high $Gd/Dy_{(n)}$. Consistency in the concentration of elements introduced by fluids, versus elements marking variable mantle depletion is explored further in Fig. 8. This shows pairs of samples, with equivalent MREE depletion, but with higher- and lower-fluid enrichment: Fig. 8a showing a sample pair from the western (non-HiMu) area and Fig. 8b a pair from eastern (HiMu) area. A less depleted sample from each area is also shown. Notably, the less depleted and depleted samples have similar levels of enrichment in the LREE, Pb and highly incompatible elements. High-fluid and low-fluid pairs in each area show amplification of Pb, Nb, Th, U and the low field strength elements, shown by the % increase columns in the upper section of each plot. Key differences between the western and eastern areas are the greater Pb enrichment in the west compared to the east, and in the stronger Nb enrichment in the east.

A viable explanation is that the *mantle wedge* contributes significantly to the Pb isotope budget of the wedge-fluid mixture. The least depleted mantle imparting more Pb (unradiogenic), and the most depleted wedge adding relatively little Pb. This is entirely possible with high mantle/fluid ratios, i.e. the fluid reacting with large mantle volumes during ascent.

Notably, the correlation between mantle depletion and enrichment is present in the western non-HiMu *and* eastern HiMu lavas. Both converge on an unradiogenic Pb ($^{206}Pb/^{204}Pb$ <18.4) in the least depleted examples (Fig. 6a), which indicates that the HiMu OIB was not an inherent part of the mantle wedge. This is also consistent with the apparent Pb isotope mixing trajectories in Fig. 5b&d. A MORB-like mantle wedge containing HiMu OIB melt or peridotite would extend the Troodos Pb isotope array towards sediment from a mixing line between MORB and HiMu OIB; i.e. along the NHRL in $^{206}Pb/^{204}Pb$–$\Delta^{207}Pb$ (Fig. 5a). As the array extends between MORB, sediment, and a point intermediate between sediment and HiMu OIB, this cannot be the case. On this basis we can conclude that the HiMu component is combined with sediment in the slab-derived hybrid fluid rather than in the mantle wedge.

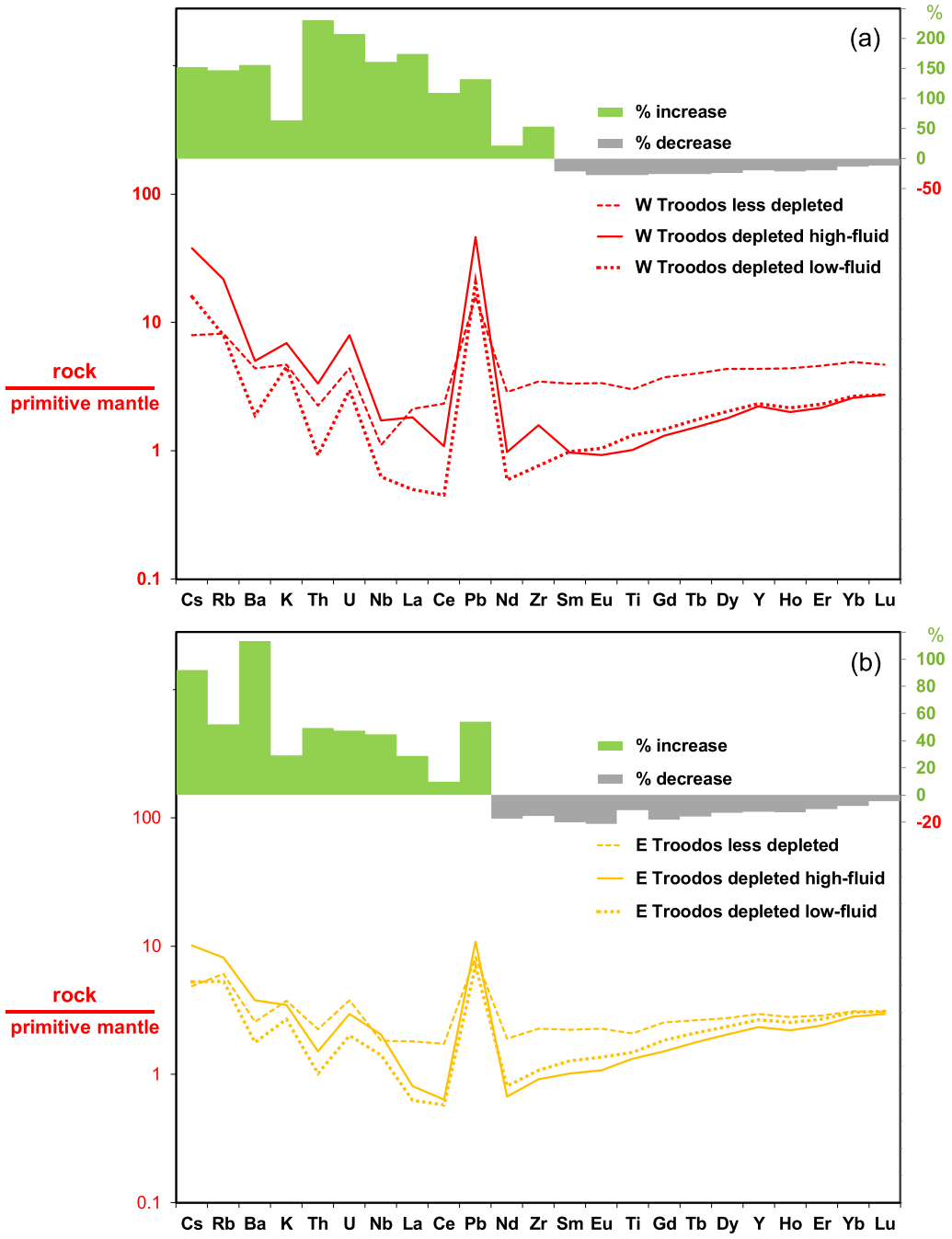

Fig. 8. (a) Incompatible element concentrations normalised to primitive mantle (Sun and McDonough, 1989) for western lavas: less depleted (sample CY102), high fluid (average of samples from Trimiklini and Yerasa, Table S1) low fluid (average of samples from Akamas). (b) Normalised concentrations for eastern lavas: less depleted (sample CY138b), high fluid (average of samples CY140, CY141, CY142 & X32a), low fluid (average of samples X84a, X81, CY134a-b-c, CY135). Bar charts above (a) and (b) show the relative concentration increase or decrease of elements between the high-fluid and low fluid-samples.

An important point about the trends produced by the western and eastern regions in Figs. 5 and 6 is that they converge at $^{206}Pb/^{204}Pb \sim 18.33$, $\Delta^{207}Pb \sim 1$, $\Delta^{208}Pb \sim 15$ and $Gd/Dy_{(n)} \sim 1$, which is indicative of a common mantle wedge component of Atlantic rather than Indian characteristics. However, it is observed in Fig. 6c that there is a large range in $\Delta^{208}Pb$ (21–49) in non-HiMu and HiMu samples with $Gd/Dy_{(n)} \sim 1$. This dispersion to high $\Delta^{208}Pb$ is more clearly displayed in the $\Delta^{207}Pb$–$\Delta^{208}Pb$ plot presented in Fig. 5e. In this "double-delta" projection, the Atlantic MORB, HiMu and sediment components are all co-linear, but Indian MORB lies to high $\Delta^{208}Pb$. Both the eastern HiMu and western non-HiMu groups form arrays extending broadly along the sediment-HiMu-Atlantic alignment, but both groups also show a dispersion towards Indian MORB compositions. As this dispersion is independent of the mantle depletion index $Gd/Dy_{(n)}$, and is consistent with the Indian MORB-rich model trajectories in Figs. 5 and 6, it points to this being a signature of subducted MORB crust. Overall, the inference is that Indian-type crust was subducted beneath Atlantic-type mantle. This is the inverse of the situation in the Western Pacific Izu-Bonin-Mariana system where Pacific/Atlantic-type crust is subducted beneath Indian-type mantle wedge (Ishizuka et al., 2020; Li et al., 2019). As such, the Troodos subduction zone marked the Cretaceous boundary between the Indian and Atlantic mantle domains.

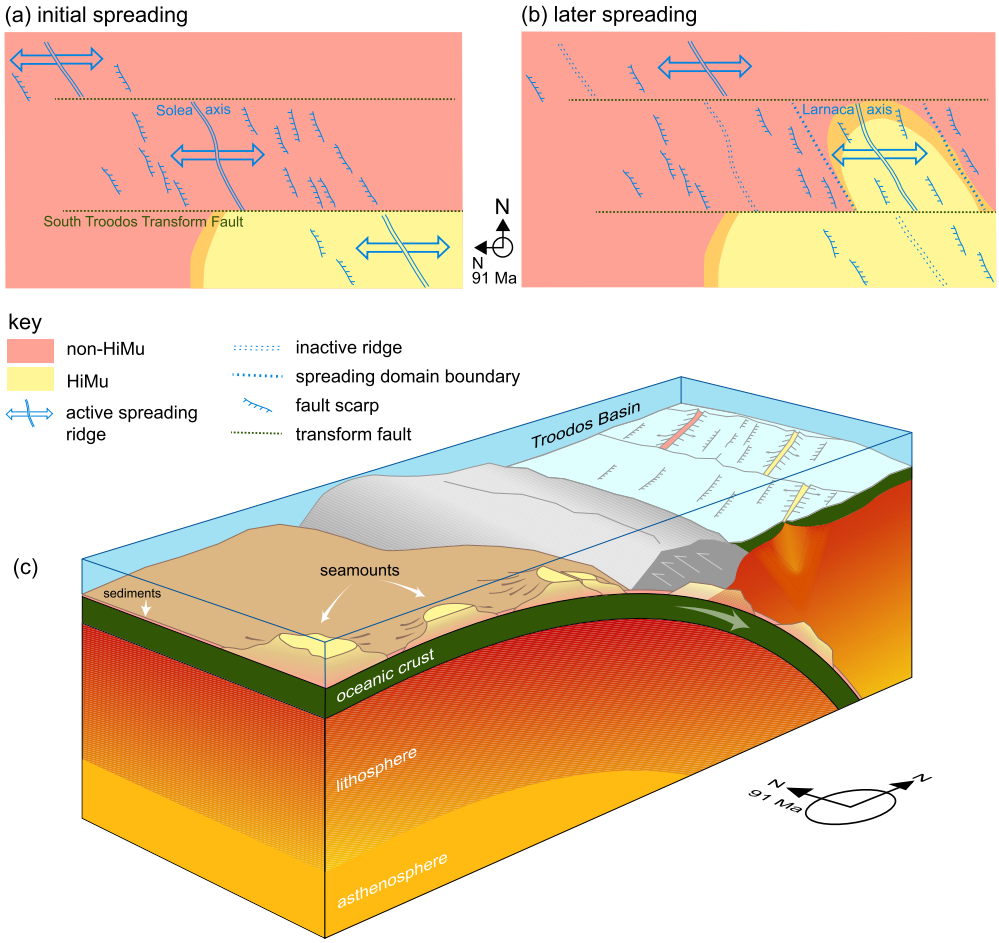

Fig. 9. Schematic tectonic reconstruction showing the evolution of spreading in the Troodos ophiolite with respect to the influence of HiMu subduction fluid. (a) Initial spreading at the Solea axis (non-HiMu) and at an axis south and east of the South Troodos Transform Fault (HiMu). (b) Spreading jumps from the Solea to Larnaca axis, generating HiMu crust north of the transform. (c) Schematic section showing spatially constrained seamount chain subduction beneath the then southern section of the Troodos Basin. Height of the block is nominally 80 km.

4.6. Seamount subduction

Observed changes in isotopic composition across the ophiolite are indicative of differences in the type of subducted material. To assess whether these reflect a temporal evolution of the slab, or are a function of the position of spreading segments relative to the subducting heterogeneity, the chemical observations are set in a tectonic framework in Fig. 9. As outlined above, sinistral ridge-offset along the South Troodos transform displaced a western ridge located north of the fault from a contemporaneous eastern ridge in the south (Fig. 9a). Crust developed as non-HiMu at the western ridge and HiMu along the eastern ridge, with the dextral slip resulting in the juxtaposition of the magma types across the transform. The postulated subsequent jump of the western ridge (Solea) to the east (Larnaca) initiated the production of HiMu crust at this new ridge location north of the fault (Fig. 9b). Therefore, it is logical that the HiMu zone of influence was a spatial phenomenon rather than a temporal evolution, and was caused by heterogeneity in the subducting crust to the southeast that persisted during the lifespan of Troodos spreading.

HiMu-like material on the east of the subducting plate is most easily reconciled as an ocean island seamount or seamount chain transported on the Neo-Tethyan oceanic crust. It is likely that this volcanic chain developed from a HiMu mantle plume that impacted close to the ridge axis of Neo-Tethys. Given the age of the HiMu Mamonia lavas, it is likely that this chain formed about 110 Ma before reaching the subduction zone. Restriction of the seamount signature to the eastern side of the ophiolite indicates that the chain subducted along a flow-line beneath this part of the Troodos fore-arc basin (Fig. 9c). It is unknown as to whether this was a complete seamount or the “feather-edge” in the form of seamount-derived volcaniclastic sediments intercalated within a pelagic sedimentary sequence. Such mixed HiMu-pelagic sedimentary sequences are a feature of the Pacific plate outboard of the Mariana arc (Hauff et al., 2003; Plank and Langmuir, 1998), while their subducted counterparts are considered to be a cause of the compositional variations along the active Izu-Bonin-Mariana arcs (Freymuth et al., 2015; Ishizuka et al., 2006; Kelley et al., 2003; Plank et al., 2007).

A foundered block which potentially represents ocean crust and/or a seamount accreted to the Troodos crust is found locked on the north side of the Cyprus trench to the southeast of the island (Welford et al., 2015a). This is the Hecataeus Rise: a ~50 km diameter block of 14–20 km thick crust with the velocity structure of thickened oceanic lithosphere (Welford et al., 2015a), which distinguishes it from the micro-continental block of the Eratosthenes seamount found to the south of the destructive plate boundary (Welford et al., 2015b). Hecataeus is capped by a similar 7 km-thick Paleogene-Neogene sedimentary sequence (Symeou et al., 2018) similar to the deposits found on the southern flank of Troodos. Late Miocene deformation along the Yerasa lineament on Cyprus is observed to continue across Hecataeus (McCallum et al., 1993). This lineament is observed on land to be a fault zone separating folded Eocene-Miocene sediments from the Cretaceous

Troodos ophiolite and overlying Moni melange. Extending this relationship offshore, and considering the chaotic seismic reflection characteristics of the pre-Eocene units, Reiche and Hubscher (2015) suggest that the Hecataeus basement could be capped by similar melange material.

5. Conclusions

A chemical transformation is identified across the Troodos crust, which reflects a spatial change in the Neo-Tethyan slab that subducted beneath the Troodos Basin. Pelagic/carbonate sediments overlying MORB were subducted beneath the west of the ophiolite, whereas in the east and south, sediment was combined with a high $^{206}Pb/^{204}Pb$ component, similar to HiMu mantle plumes distributed around northern Africa. This switch in character is proposed to represent a progressive change in the location of supra-subduction spreading relative to the path of a seamount chain colliding with, and subducting beneath, the Troodos trench. The Hecataeus Rise, located to the current southeast of Cyprus, is a candidate to be a foundered relic of this seamount chain, locked in the subduction zone.

Both the sediment-rich and HiMu-rich components impart their Pb isotope signature via subduction fluid fluxing of the mantle wedge. While Pb enrichment from subduction is relatively consistent, the Pb isotope composition of lavas generally correlates with the degree of melt depletion their mantle source had experienced. This indicates that the mantle wedge also significantly contributed to the Pb isotope signature, imparting its Atlantic/Pacific mantle characteristics. Isotopic evidence also points to the involvement of subducted ocean crust, which imparted a signature consistent with an origin at a spreading centre with Indian Ocean mantle characteristics.

Lavas from both the sediment- and HiMu-influenced domains also show a variation in the amount of subduction fluid component regardless of depletion. More fluid-enriched samples shifting Pb and Nd isotope compositions towards their appropriate domain signatures. However, along with the enrichment of Rb, Ba, K, Th and U, the greater addition of sediment and HiMu fluids also enhances Nb: an effect most apparent in the eastern HiMu-domain which is spatially characterised by low Th/Nb. This can be modelled to originate from the significantly higher Nb found in HiMu lavas relative to sediments on the subducted slab.

CRediT authorship contribution statement

RNT wrote the manuscript, RNT and OI conducted fieldwork, all authors contributed to the analyses and to discussion of the results.

Declaration of competing interest

The authors declare no competing interests.

Acknowledgements

The authors wish to thank Cyprus Geological Survey for assistance in the field. Andy Milton and Matt Cooper are thanked for laboratory excellence. Taylor thanks NERC (UK) for grant NE/M012034/1 and Ishizuka and Taylor thank JSPS KAKENHI grant JP25287133. This work has benefited from discussions with Bram Murton, Julian Pearce and Martin Palmer. Mark Reagan and two anonymous reviewers are thanked for improving the manuscript.

Appendix A. Supplementary material

Supplementary material related to this article can be found online at https://doi.org/10.1016/j.epsl.2022.117509.

References

Abelson, M., Baer, G., Agnon, A., 2002. Fossil ridge-transform intersection in the Troodos ophiolite: new perspectives from rock magnetism in the gabbro suite and fracture mechanics analysis. Geochem. Geophys. Geosyst. 3.
Allerton, S., 1989. Distortions, rotations and crustal thinning at ridge–transform intersections. Nature 340, 626–628.
Allerton, S., Vine, F.J., 1987. Spreading structure of the Troodos ophiolite, Cyprus: some paleomagnetic constraints. Geology 15, 593–597.
Allerton, S., Vine, F.J., 1991. Spreading evolution of the Troodos ophiolite, Cyprus. Geology 19, 637–640.
Bear, L., 1960. Cyprus geological survey department memoir 3. In: The Geology and Mineral Resources of the Akaki-Lythrodondha Area. Government of Cyprus, Nicosia, Cyprus, p. 122.
Cameron, W.E., 1985. Petrology and origin of primitive lavas from the Troodos ophiolite, Cyprus. Contrib. Mineral. Petrol. 89, 239–255.
Chauvet, F., Lapierre, H., Maury, R.C., Bosch, D., Basile, C., Cotten, J., Brunet, P., Campillo, S., 2011. Triassic alkaline magmatism of the Hawasina Nappes: post-breakup melting of the Oman lithospheric mantle modified by the Permian Neotethyan Plume. Lithos 122, 122–136.
Coogan, L.A., Banks, G.J., Gillis, K.M., MacLeod, C.J., Pearce, J.A., 2003. Hidden melting signatures recorded in the Troodos ophiolite plutonic suite: evidence for widespread generation of depleted melts and intra-crustal melt aggregation. Contrib. Mineral. Petrol. 144, 484–505.
Cooke, A.J., Masson, L.P., Robertson, A.H.F., 2014. Construction of a sheeted dyke complex: evidence from the northern margin of the Troodos Ophiolite and its southern margin adjacent to the Arakapas Fault Zone. Ofioliti 39, 1–30.
Cooper, L.B., Plank, T., Arculus, R.J., Hauri, E.H., Hall, P.S., Parman, S.W., 2010. High-Ca boninites from the active Tonga Arc. J. Geophys. Res., Solid Earth 115.
Deniel, C., Vidal, P., Coulon, C., Vellutini, P.-J., Piguet, P., 1994. Temporal evolution of mantle sources during continental rifting: the volcanism of Djibouti (Afar). J. Geophys. Res., Solid Earth 99, 2853–2869.
Escrig, S., Bezos, A., Langmuir, C.H., Michael, P.J., Arculus, R., 2012. Characterizing the effect of mantle source, subduction input and melting in the Fonualei Spreading Center, Lau Basin: constraints on the origin of the boninitic signature of the back-arc lavas. Geochem. Geophys. Geosyst. 13.
Falloon, T.J., Danyushevsky, L.V., Crawford, A.J., Meffre, S., Woodhead, J.D., Bloomer, S.H., 2008. Boninites and adakites from the northern termination of the Tonga trench: implications for adakite petrogenesis. J. Petrol. 49, 697–715.
Fonseca, R.O.C., Kirchenbaur, M., Ballhaus, C., Munker, C., Zirner, A., Gerdes, A., Heuser, A., Botcharnikov, R., Lenting, C., 2017. Fingerprinting fluid sources in Troodos ophiolite complex orbicular glasses using high spatial resolution isotope and trace element geochemistry. Geochim. Cosmochim. Acta 200, 145–166.
Freymuth, H., Vils, F., Willbold, M., Taylor, R.N., Elliott, T., 2015. Molybdenum mobility and isotopic fractionation during subduction at the Mariana arc. Earth Planet. Sci. Lett. 432, 176–186.
Gale, N.H., StosGale, Z.A., Maliotis, G., Annetts, N., 1997. Lead isotope data from the Isotrace Laboratory, Oxford: archaeometry data base 4, ores from Cyprus. Archaeometry 39, 237–246.
Gass, I., MacLeod, C., Murton, B., Panayiotou, A., Simonian, K., Xenophontos, C., 1994. The Geological Evolution of the Southern Troodos Transform Fault Zone, Cyprus, vol. 9. Geological Survey Department.
Gass, I., 1960. The geology and mineral resources of the Dhali area. Authority of the Government of Cyprus.
Gass, I.G., 1968. Is the Troodos Massif of Cyprus a fragment of Mesozoic Ocean Floor? Nature 220, 39–42.
Geldmacher, J., Hoernle, K., 2000. The 72 Ma geochemical evolution of the Madeira hotspot (eastern North Atlantic): recycling of Paleozoic (<= 500 Ma) oceanic lithosphere. Earth Planet. Sci. Lett. 183, 73–92.
Geldmacher, J., Hoernle, K., Klügel, A., Bogaard, P.v.d., Wombacher, F., Berning, B., 2006. Origin and geochemical evolution of the Madeira-Tore Rise (eastern North Atlantic). J. Geophys. Res., Solid Earth 111.
Haase, K.M., Beier, C., Kemner, F., 2019. A comparison of the magmatic evolution of Pacific intraplate volcanoes: constraints on melting in mantle plumes. Front. Earth Sci. 6.
Hart, S.R., 1984. A large-scale isotope anomaly in the southern hemisphere mantle. Nature 309, 753–757.
Hauff, F., Hoernle, K., Schmidt, A., 2003. Sr-Nd-Pb composition of Mesozoic Pacific oceanic crust (Site 1149 and 801, ODP Leg 185): Implications for alteration of ocean crust and the input into the Izu-Bonin-Mariana subduction system. Geochem. Geophys. Geosyst. 4.
Hickey-Vargas, R., Yogodzinski, G.M., Ishizuka, O., McCarthy, A., Bizimis, M., Kusano, Y., Savov, I.P., Arculus, R., 2018. Origin of depleted basalts during subduction initiation and early development of the Izu-Bonin-Mariana island arc: evidence from IODP expedition 351 site U1438, Amami-Sankaku basin. Geochim. Cosmochim. Acta 229, 85–111.
Ishizuka, O., Taylor, R.N., Milton, J.A., Nesbitt, R.W., Yuasa, M., Sakamoto, I., 2006. Variation in the mantle sources of the northern Izu arc with time and space - constraints from high-precision Pb isotopes. J. Volcanol. Geotherm. Res. 156, 266–290.

Ishizuka, O., Taylor, R.N., Umino, S., Kanayama, K., 2020. Geochemical evolution of arc and slab following subduction initiation: a record from the Bonin Islands, Japan. J. Petrol. 61.
Ishizuka, O., Umino, S., Taylor, R.N., Kanayama, K., 2014. Evidence for hydrothermal activity in the earliest stages of intraoceanic arc formation: implications for ophiolite-hosted hydrothermal activity. Econ. Geol. 109, 2159–2177.
Kelley, K.A., Plank, T., Ludden, J., Staudigel, H., 2003. Composition of altered oceanic crust at ODP Sites 801 and 1149. Geochem. Geophys. Geosyst. 4.
Kessel, R., Schmidt, M.W., Ulmer, P., Pettke, T., 2005. Trace element signature of subduction-zone fluids, melts and supercritical liquids at 120–180 km depth. Nature 437, 724–727.
Klaver, M., Davies, G.R., Vroon, P.Z., 2016. Subslab mantle of African provenance infiltrating the Aegean mantle wedge. Geology 44, 367–370.
Klaver, M., Djuly, T., de Graaf, S., Sakes, A., Wijbrans, J., Davies, G., Vroon, P., 2015. Temporal and spatial variations in provenance of eastern Mediterranean Sea sediments: implications for Aegean and Aeolian arc volcanism. Geochim. Cosmochim. Acta 153, 149–168.
Konig, S., Munker, C., Schuth, S., Garbe-Schonberg, D., 2008. Mobility of tungsten in subduction zones. Earth Planet. Sci. Lett. 274, 82–92.
Konig, S., Munker, C., Schuth, S., Luguet, A., Hoffmann, J.E., Kuduon, J., 2010. Boninites as windows into trace element mobility in subduction zones. Geochim. Cosmochim. Acta 74, 684–704.
Koppers, A.A.P., Staudigel, H., Wijbrans, J.R., Pringle, M.S., 1998. The Magellan seamount trail: implications for Cretaceous hotspot volcanism and absolute Pacific plate motion. Earth Planet. Sci. Lett. 163, 53–68.
Kostopoulos, D., Murton, B., 1992. Origin and distribution of components in boninite genesis: significance of the OIB component. Geol. Soc. (Lond.) Spec. Publ. 60, 133–154.
Lapierre, H., Bosch, D., Narros, A., Mascle, G.H., Tardy, M., Demant, A., 2007. The Mamonia Complex (SW Cyprus) revisited: remnant of Late Triassic intra-oceanic volcanism along the Tethyan southwestern passive margin. Geol. Mag. 144, 1–19.
Lapierre, H., Samper, A., Bosch, D., Maury, R., Bechennec, F., Cotten, J., Demant, A., Brunet, P., Keller, F., Marcoux, J., 2004. The Tethyan plume: geochemical diversity of Middle Permian basalts from the Oman rifted margin. Lithos 74, 167–198.
Li, H.Y., Taylor, R.N., Prytulak, J., Kirchenbaur, M., Shervais, J.W., Ryan, J.G., Godard, M., Reagan, M.K., Pearce, J.A., 2019. Radiogenic isotopes document the start of subduction in the Western Pacific. Earth Planet. Sci. Lett. 518, 197–210.
Mackenzie, G.D., Maguire, P.K.H., Coogan, L.A., Khan, M.A., Eaton, M., Petrides, G., 2006. Geophysical constraints on the crustal architecture of the Troodos ophiolite: results from the IANGASS project. Geophys. J. Int. 167, 1385–1401.
MacLeod, C.J., Allerton, S., Gass, I.G., Xenophontos, C., 1990. Structure of a fossil ridge–transform intersection in the Troodos ophiolite. Nature 348, 717–720.
Maffione, M., van Hinsbergen, D.J.J., de Gelder, G., van der Goes, F.C., Morris, A., 2017. Kinematics of Late Cretaceous subduction initiation in the Neo-Tethys Ocean reconstructed from ophiolites of Turkey, Cyprus, and Syria. J. Geophys. Res., Solid Earth 122, 3953–3976.
Mahoney, J.J., Frei, R., Tejada, M.L.G., Mo, X.X., Leat, P.T., Nagler, T.F., 1998. Tracing the Indian Ocean mantle domain through time: Isotopic results from Old West Indian, East Tethyan, and South Pacific seafloor. J. Petrol. 39, 1285–1306.
Martin, A.J., Keith, M., McDonald, I., Haase, K.M., McFall, K.A., Klemd, R., MacLeod, C.J., 2019. Trace element systematics and ore-forming processes in mafic VMS deposits: evidence from the Troodos ophiolite, Cyprus. Ore Geol. Rev. 106, 205–225.
McCallum, J.E., Scrutton, R.A., Robertson, A.H.F., Ferrari, W., 1993. Seismostratigraphy and Neogene-Recent depositional history of the south central continental margin of Cyprus. Mar. Pet. Geol. 10, 426–438.
Meyzen, C.M., Blichert-Toft, J., Ludden, J.N., Humler, E., Mevel, C., Albarede, F., 2007. Isotopic portrayal of the Earth's upper mantle flow field. Nature 447, 1069–1074.
Moores, E.M., Robinson, P.T., Malpas, J., Xenophonotos, C., 1984. Model for the origin of the Troodos massif, Cyprus, and other mideast ophiolites. Geology 12, 500–503.
Moores, E.M., Varga, R.J., Verosub, K.L., Ramsden, T., 1990. Regional structure of the Troodos dyke complex. In: Malpas, J.G., Moores, E.M., Panayiotou, A., Xenophontos, X. (Eds.), Ophiolites and Oceanic Analogues, Proceedings of Symposium Troodos 1987. Geological Survey Department, Ministry of Agriculture and Natural Resources, Cyprus, pp. 27–35.
Morris, A., Creer, K.M., Robertson, A.H.F., 1990. Palaeomagnetic evidence for clockwise rotations related to dextral shear along the Southern Troodos Transform Fault, Cyprus. Earth Planet. Sci. Lett. 99, 250–262.
Morris, A., Maffione, M., 2016. Is the Troodos ophiolite (Cyprus) a complete, transform fault-bounded Neotethyan ridge segment? Geology 44, 199–202.
Nuccio, P.M., Paonita, A., Rizzo, A., Rosciglione, A., 2008. Elemental and isotope covariation of noble gases in mineral phases from Etnean volcanics erupted during 2001-2005, and genetic relation with peripheral gas discharges. Earth Planet. Sci. Lett. 272, 683–690.
Pearce, J.A., Kempton, P.D., Nowell, G.M., Noble, S.R., 1999. Hf-Nd element and isotope perspective on the nature and provenance of mantle and subduction components in Western Pacific arc-basin systems. J. Petrol. 40, 1579–1611.
Pearce, J.A., Lippard, S.J., Roberts, S., 1984. Characteristics and tectonic significance of supra-subduction zone ophiolites. Geol. Soc. (Lond.) Spec. Publ. 16, 77–94.
Pearce, J.A., Reagan, M.K., 2019. Identification, classification, and interpretation of boninites from Anthropocene to Eoarchean using Si-Mg-Ti systematics. Geosphere 15, 1008–1037.
Pearce, J.A., Robinson, P.T., 2010. The Troodos ophiolitic complex probably formed in a subduction initiation, slab edge setting. Gondwana Res. 18, 60–81.
Peate, D.W., Pearce, J.A., 1998. Causes of spatial compositional variations in Mariana arc lavas: trace element evidence. Isl. Arc 7, 479–495.
Plank, T., Kelley, K.A., Murray, R.W., Stern, L.Q., 2007. Chemical composition of sediments subducting at the Izu-Bonin trench. Geochem. Geophys. Geosyst. 8.
Plank, T., Langmuir, C.H., 1998. The chemical composition of subducting sediment and its consequences for the crust and mantle. Chem. Geol. 145, 325–394.
Rautenschlein, M., Jenner, G.A., Hertogen, J., Hofmann, A.W., Kerrich, R., Schmincke, H.U., White, W.M., 1985. Isotopic and trace element composition of volcanic glasses from the Akaki Canyon, Cyprus: implications for the origin of the Troodos ophiolite. Earth Planet. Sci. Lett. 75, 369–383.
Reiche, S., Hubscher, C., 2015. The Hecataeus Rise, easternmost Mediterranean: a structural record of Miocene-Quaternary convergence and incipient continent-continent-collision at the African-Anatolian plate boundary. Mar. Pet. Geol. 67, 368–388.
Robertson, A., Xenophontos, C., 1993. Development of concepts concerning the Troodos ophiolite and adjacent units in Cyprus. Geol. Soc. (Lond.) Spec. Publ. 76, 85–119.
Rodrigo-Gamiz, M., Martinez-Ruiz, F., Chiaradia, M., Jimenez-Espejo, F.J., Ariztegui, D., 2015. Radiogenic isotopes for deciphering terrigenous input provenance in the western Mediterranean. Chem. Geol. 410, 237–250.
Rooney, T.O., Hanan, B.B., Graham, D.W., Furman, T., Blichert-Toft, J., Schilling, J.G., 2012. Upper mantle pollution during Afar Plume-Continental Rift interaction. J. Petrol. 53, 365–389.
Schilling, J.-G., Kingsley, R.H., Hanan, B.B., McCully, B.L., 1992. Nd-Sr-Pb isotopic variations along the Gulf of Aden: evidence for Afar mantle plume-continental lithosphere interaction. J. Geophys. Res. 97, 10927–10966.
Scott, C.P., Titus, S.J., Davis, J.R., 2013. Using field data to constrain a numerical kinematic model for ridge-transform deformation in the Troodos ophiolite, Cyprus. Lithosphere 5, 109–127.
Shen, F.Y., Niu, Y.L., Chen, Y.H., Gao, Y.J., Wang, X.H., Duan, M., Shan, L., 2020. Origin of magmatic harzburgite as a result of boninite magma evolution - an illustration using layered harzburgite-dunite cumulate from the Troodos ophiolite complex. Lithos 376.
Stos-Gale, Z.A., Gale, N.H., 2009. Metal provenancing using isotopes and the Oxford archaeological lead isotope database (OXALID). Archaeol. Anthropol. Sci. 1, 195–213.
Sun, S.-s., McDonough, W.F., 1989. Chemical and isotopic systematics of oceanic basalts: implications for mantle composition and processes. Geol. Soc. (Lond.) Spec. Publ. 42, 313–345.
Symeou, V., Homberg, C., Nader, F.H., Darnault, R., Lecomte, J.C., Papadimitriou, N., 2018. Longitudinal and temporal evolution of the tectonic style along the Cyprus arc system, assessed through 2-D reflection seismic interpretation. Tectonics 37, 30–47.
Tamura, Y., Tani, K., Chang, Q., Shukuno, H., Kawabata, H., Ishizuka, O., Fiske, R.S., 2007. Wet and dry basalt magma evolution at Torishima Volcano, iZu–Bonin Arc, Japan: the possible role of phengite in the downgoing slab. J. Petrol. 48, 1999–2031.
Taylor, R.N., 1990. Geochemical stratigraphy of the Troodos extrusive sequence; temporal developments of a spreading centre magma chamber. In: Malpas, J.G., Moores, E.M., Panayiotou, A., Xenophontos, X. (Eds.), Ophiolites and Oceanic Analogues, Proceedings of Symposium Troodos 1987. Geological Survey Department, Ministry of Agriculture and Natural Resources, Cyprus, pp. 173–184.
Taylor, R.N., Davila-Harris, P., Branney, M.J., Ruth Farley, E.M., Gernon, T.M., Palmer, M.R., 2020. Dynamics of a chemically pulsing mantle plume. Earth Planet. Sci. Lett. 537, 116182.
Taylor, R.N., Ishizuka, O., Michalik, A., Milton, J.A., Croudace, I.W., 2015. Evaluating the precision of Pb isotope measurement by mass spectrometry. J. Anal. At. Spectrom. 30, 198–213.
Taylor, R.N., Murton, B.J., Nesbitt, R.W., 1992. Chemical transects across intra-oceanic arcs: implications for the tectonic setting of ophiolites. Geol. Soc. (Lond.) Spec. Publ. 60, 117–132.
Taylor, R.N., Nesbitt, R.W., 1988. Light rare-earth enrichment of supra subduction-zone mantle: evidence from the Troodos ophiolite, Cyprus. Geology 16, 448–451.
Thy, P., Brooks, C.K., Walsh, J.N., 1985. Tectonic and petrogenetic implications of major and rare earth element chemistry of Troodos glasses, Cyprus. Lithos 18, 165–178.
Thy, P., Esbensen, K.H., 1993. Seafloor spreading and the ophiolitic sequences of the Troodos Complex: a principal component analysis of lava and dike compositions. J. Geophys. Res., Solid Earth 98, 11799–11805.
Timm, C., Graham, I.J., de Ronde, C.E.J., Leybourne, M.I., Woodhead, J., 2011. Geochemical evolution of Monowai volcanic center: new insights into the northern Kermadec arc subduction system, SW Pacific. Geochem. Geophys. Geosyst. 12.
van Everdingen, D.A., 1995. Fracture characteristics of the Sheeted Dike Complex, Troodos ophiolite, Cyprus: implications for permeability of oceanic crust. J. Geophys. Res., Solid Earth 100, 19957–19972.

Varga, R.J., Moores, E.M., 1985. Spreading structure of the Troodos ophiolite, Cyprus. Geology 13, 846–850.

Wang, Y., Han, X., Petersen, S., Frische, M., Qiu, Z., Cai, Y., Zhou, P., 2018. Trace metal distribution in sulfide minerals from ultramafic-hosted hydrothermal systems: examples from the Kairei Vent field, Central Indian Ridge. Minerals 8 (11), 526. https://doi.org/10.3390/min8110526.

Welford, J.K., Hall, J., Hubscher, C., Reiche, S., Louden, K., 2015a. Crustal seismic velocity structure from Eratosthenes Seamount to Hecataeus Rise across the Cyprus Arc, eastern Mediterranean. Geophys. J. Int. 200, 933–951.

Welford, J.K., Hall, J., Rahimi, A., Reiche, S., Hubscher, C., Louden, K., 2015b. Crustal structure from the Hecataeus Rise to the Levantine Basin, eastern Mediterranean, from seismic refraction and gravity modelling. Geophys. J. Int. 203, 2055–2069.

White, W.M., 2020. Geochemistry. John Wiley & Sons.

Woelki, D., Regelous, M., Haase, K.M., Beier, C., 2019. Geochemical mapping of a paleo-subduction zone beneath the Troodos Ophiolite. Chem. Geol. 523, 1–8.

Woelki, D., Regelous, M., Haase, K.M., Romer, R.H.W., Beier, C., 2018. Petrogenesis of boninitic lavas from the Troodos Ophiolite, and comparison with Izu-Bonin-Mariana fore-arc crust. Earth Planet. Sci. Lett. 498, 203–214.

Woelki, D., Michael, P.J., Regelous, M., Haase, K.M., 2020. Enrichment of H_2O and fluid-soluble trace elements in the Troodos a far Ophiolite: evidence for a near-trench origin. Lithos 356.

Woodhead, J., Hergt, J., Greig, A., Edwards, L., 2011. Subduction zone Hf-anomalies: mantle messenger, melting artefact or crustal process? Earth Planet. Sci. Lett. 304, 231–239.

Workman, R.K., Hart, S.R., 2005. Major and trace element composition of the depleted MORB mantle (DMM). Earth Planet. Sci. Lett. 231, 53–72.

Zhang, S.Q., Mahoney, J.J., Mo, X.X., Ghazi, A.M., Milani, L., Crawford, A.J., Guo, T.Y., Zhao, Z.D., 2005. Evidence for a widespread Tethyan upper mantle with Indian-Ocean-type isotopic characteristics. J. Petrol. 46, 829–858.

Zindler, A., Hart, S., 1986. Chemical geodynamics. Annu. Rev. Earth Planet. Sci. 14, 493–571.